Determination of instantaneous pressure in an axisymmetric base flow using time-resolved tomographic PIV

P.L. Blinde, V. Gentile, B.W. van Oudheusden and F.F.J. Schrijer

Delft University of Technology, Faculty of Aerospace Engineering, The Netherlands

1 Introduction

Quantification of mean and fluctuating surface loads is critical for the efficient design of aerospace structures. To measure surface pressure in experiments, wind tunnel models are typically equipped with pressure transducers, which offer high sampling rates and high sensitivity. In order to have a sufficient spatial sampling of the surface pressure such that the instantaneous surface loads can be determined, a large number of transducers is required. From a practical point of view, the installation of transducers can be costly and can pose significant challenges due to spatial limitations inside the wind tunnel model.

An alternative for measuring pressure is PIV-based pressure determination [1]. In this approach, PIV data are used to determine the material acceleration, which is related to the local pressure gradient via the momentum equation. Whereas the mean pressure field can be obtained from a series of uncorrelated velocity fields (e.g. [2]), the availability of time-resolved PIV data allow for the determination of instantaneous pressure fields. Recent developments in PIV measurement capabilities, in particular tomographic PIV [3], have made this technique increasingly feasible and appealing. A particular advantage of the technique is that it provides simultaneous velocity and pressure data in the full flow field, thus enabling a better understanding of the relation between fluid dynamics and the corresponding pressure field.

The ability of PIV to determine the material acceleration, from which the pressure can subsequently be obtained, has been the subject of extensive study. Using two or more velocity fields closely separated in time, the material acceleration can be determined using traditional Eulerian or Lagrangian formulations (see e.g. [1] for details). An improved estimate of the material acceleration may be obtained using fluid trajectory tracking (FTC) which correlates more than two consecutive reconstructions [4, 5].

The present study builds on these efforts by using time-resolved tomographic PIV to obtain instantaneous pressure distributions in a low-speed axisymmetric base flow. Results are compared to simultaneous unsteady pressure measurements using microphones and mean pressure measurements using static pressure sensors.

2 Experimental arrangements and measurement techniques

The measurements were conducted in the low-speed wind tunnel (W-Tunnel) of the Aerodynamics Laboratories of Delft University of Technology. The freestream velocity (U_∞) of the flow is 10 m/s and the Reynolds number based on the model diameter (Re_D) is about 35,000.

The model is an ogive-cylinder with a diameter (D) of 50 mm equipped with an afterbody with a diameter of 20 mm (0.4 D) (see Figure 1). The length of the after-body is 90 mm (i.e. 1.8 D). The afterbody contains pinholes with a spacing of 10 mm (0.2 D) for measurements of pressure fluctuations via microphones and of the mean pressure using static pressure ports. For brevity, these measurements are not discussed in detail in this paper. The model is supported by a wing-shaped airfoil (NACA 0018, 60 mm chord length). Transition of the incoming boundary layer to the turbulent regime is forced in the upstream part of the model by randomly distributed carborundum particles with a mean diameter of 0.8 mm on an 8 mm wide strip [6].

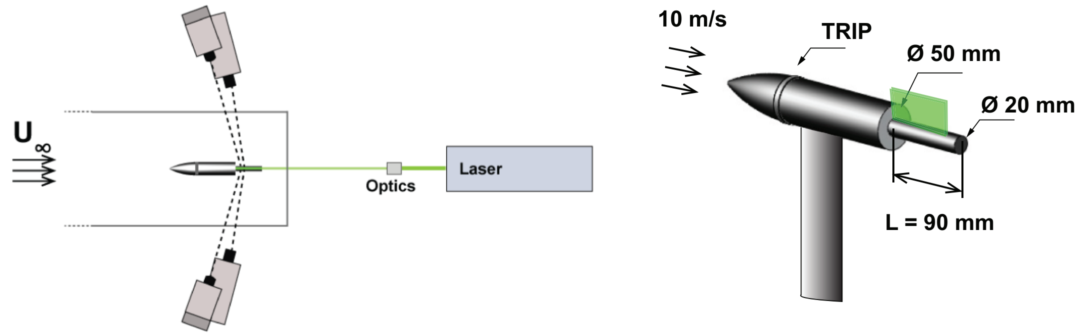

Fig. 1. Experimental setup, top view (left); wind-tunnel model (right).

The PIV measurements are performed in a thin volume located downstream of the step over the afterbody surface where the pressure transducers are located (see figure 1). The size of the measurement volume is 1.5D × 0.7D × 0.07 D (75 mm × 35 mm × 3.5 mm, L × H × W). The flow is uniformly seeded by a SAFEX smoke generator with tracers of 1 µm. The typical seeding concentration is 0.05 particles per pixel (ppp). Illumination is provided by a Quantronix Darwin Duo Nd-YLF laser (2 x 25 mJ/pulse at 1 kHz), placed downstream and below the test section. The laser beam impinges the model base after being shaped to into a light sheet with a thickness of about 4 mm. Particle images are recorded by four Photron FastCAM SA1.1 CMOS cameras (maximum resolution 1024 x 1024 pixels, 20 µm pixel pitch) placed at opposite sites of the test section. All cameras are placed at a yaw angle of about 30° to receive forward scattered light. Two cameras, equipped with a 60 mm Nikon objectives, are located at the same height as the base of the model at either side of the field of view. The two other cameras are placed to view from above at a pitch angle of about 40°. These cameras are equipped with 105 mm Nikon objective. The objectives are installed on a tilt mechanism to satisfy the Scheimpflug condition and their aperture is set to $f_{\#}$ = 5.6. The magnification is 0.25 and the resulting digital resolution is 12.3 pixel mm^{-1}.

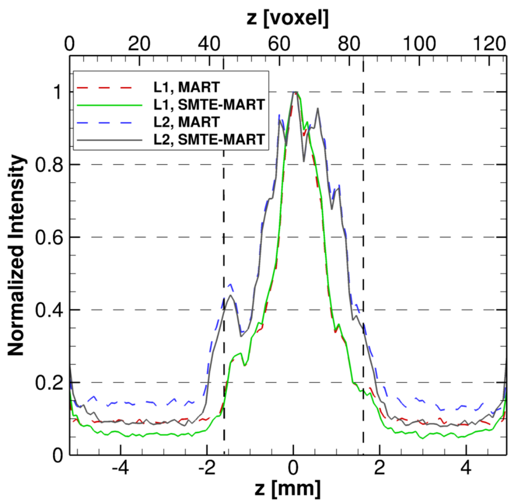

Fig. 2. Representative reconstructed normalized intensity profiles for laser pulses L1 and L2. Dashed vertical lines indicate the boundaries for the measurement volume

Images of 1024 x 512 pixels are recorded at 10 kHz in single-frame mode, leading to a time separation of 100 µs., corresponding to a maximum particle displacement of 10 pixels. The recordings consist of 10,941 images over a time span of about 1.0 second.

Particle images are pre-processed by subtracting the local minimum intensity over a 15 images-sized kernel and subtracting the minimum intensity within 31 pixel-sized kernels. Gaussian smoothing and sharpening is applied to reduce noise. The particle image size after smoothing/sharpening is about 2.2 pixels.

Reconstructed volumes are obtained using the SMTE-MART algorithm [7] performed by in-house software (Fluere). The resulting reconstructions have a signal-to-noise ration (SNR) of about 10 (see Figure 2). 10 MART iterations are performed using 3 × 3 × 3 Gaussian smoothing after each iteration, excluding the final iteration. The computations are optimized by not updating voxels with an intensity below 0.01 counts [8].

Cross-correlation of the reconstructed objects is performed using iterative volume deformation, symmetric block direct correlation [9] and Gaussian window weighting. Spurious vectors are identified by universal outlier detection [10] and replaced using linear interpolation. Intermediate vector fields are smoothed before use in the next iteration. The final interrogation volumes have a size of 20 × 20 × 20 voxels so that each volume contains approximately 8 particles. With a 75% window overlap the resulting vector spacing is 0.41 mm. The resulting velocity fields are used as predictor for the FTC algorithm [4] which is implemented here to converge to a least-square 2nd-order polynomial fit through a 5-timestep particle pattern trajectory via 2 iterations.

The instantaneous pressure is obtained from the velocity fields via the momentum equation for inviscid flow (eq. 1).

$$\nabla p = -\rho \frac{D\boldsymbol{u}}{Dt} \qquad (1)$$

where p is the static pressure, ρ the density and D**u**/Dt the material acceleration which is obtained from the PIV velocity data on the basis of a 1st-order least-square fit through velocities along imaginary particle tracks over 5 snapshots (see [11]). These tracks have been reconstructed using linear interpolation in combination with a 2nd-order accurate integration, while ensuring that the CFL condition is met throughout the domain. Equation (1) is then solved for pressure by first casting it into a Poisson equation (see e.g. [11–14]), which is then discretized using a second-order finite difference scheme. Pressure gradients are prescribed as Neumann boundary conditions used on all sides of the domain except for the top, where the pressure as obtained from the isentropic flow relation (Bernoulli equation) is prescribed as Dirichlet boundary condition. The resulting linear system is solved using the Matlab algorithm *mldivide*.

3 Results

Figure 3 shows contour plots of an example instantaneous velocity field and of the mean velocity field (streamwise component) and turbulence intensity defined as the RMS of velocity fluctuations. The flow is characterized by a large-scale separated region, with reattachment occurring at approximately x/D = 0.9. Within the separated region, backflow is present with a magnitude of up to 30% of the freestream velocity.

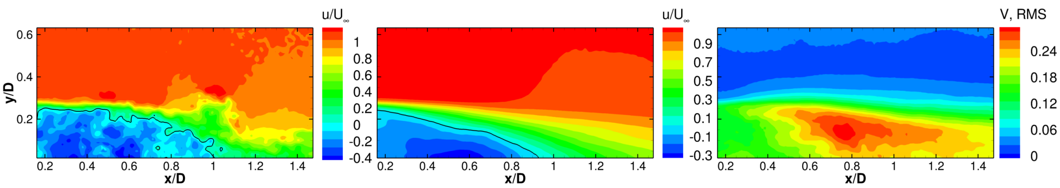

Fig. 3. Instantaneous velocity field, u component (left). Mean velocity field, u-component (centre). Turbulence intensity (right)

Figure 4 shows the corresponding instantaneous pressure field, the mean pressure field and RMS pressure field. The two left figures shows a pressure organization with lower pressure in the upstream part of the measurement volume and higher pressure in the downstream part of the field of view. The low pressure region can be associated to the recirculation region (compare Figure 4). The RMS pressure field (right) shows maximum values in the shear layer and at reattachment.

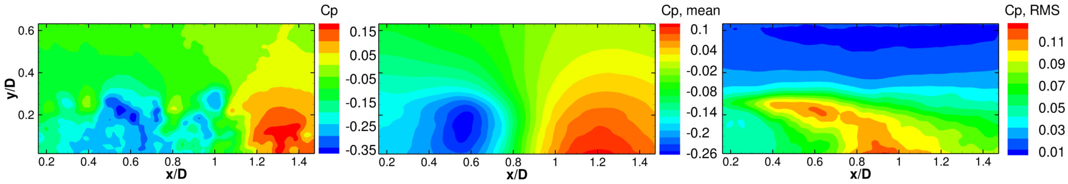

Fig. 4. Instantaneous pressure field (left). Mean pressure field (centre). RMS pressure field (right)

To assess the PIV results, Figure 5 compares the mean pressure (left figure) and RMS of pressure fluctuations (right figure) measured by the sensors in the afterbody and the results obtained by PIV. Results from similar studies reported in literature [15–18] have been included in the comparison. The mean pressure profile from PIV shows good agreement with the pressure sensors. The RMS pressure profile is however much higher than the fluctuations as measured by microphones and as reported in literature.

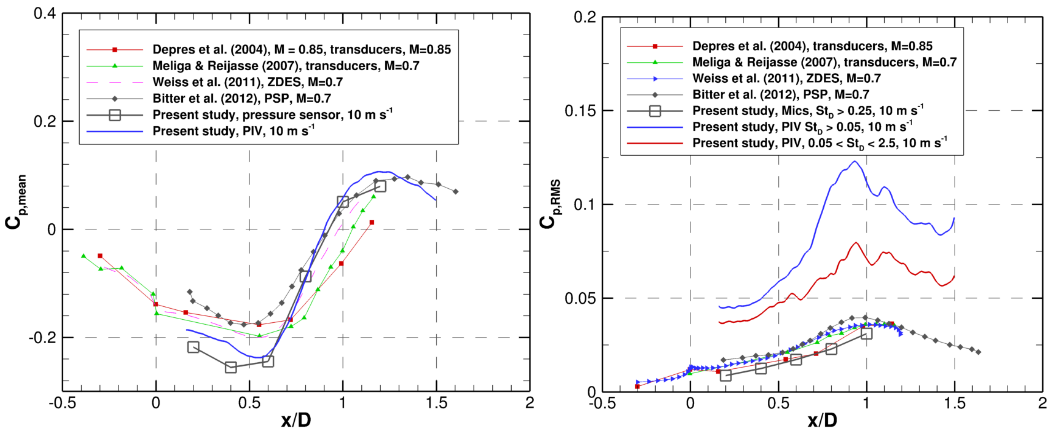

Fig. 5. Mean pressure profile (left). RMS pressure profile (right)

4 Conclusions

Time-resolved, tomographic PIV measurements downstream an axisymmetric step were used to reconstruct instantaneous pressure fields. Microphone measurements and static pressure measurements were used to provide in-situ validation. The mean PIV-based mean pressure showed reasonable agreement with these reference measurements and with values reported in literature. The pressure fluctuations obtained from PIV were however found to be substantially higher. From this comparison, it is concluded that the present PIV-based pressure determination procedure requires improvements to obtain more reliable pressure data.

Acknowledgements

This work is supported by the European FP-7 project “NIOPLEX”, grant agreement 605151.

References

1. Van Oudheusden, B.W., PIV-based pressure measurement. Meas. Sci. Technol. **24** (2013).
2. Van Oudheusden, B.W., Scarano, F., Roosenboom, E.W.M., Casimiri, E.W.F., Souverein, L.J., Evaluation of integral forces and pressure fields from planar velocimetry data for incompressible and compressible flows. Exp. Fluids. **43** (2007).
3. Scarano, F., Tomographic PIV: principles and practice. Meas. Sci. Technol. **24** (2013).
4. Lynch, K.P., Scarano, F., A high-order time-accurate interrogation method for time-resolved PIV. Meas. Sci. Technol. **24** (2013).
5. Lynch, K.P., Scarano, F., Material acceleration estimation by four-pulse tomo-PIV. Meas. Sci. Technol. **25** (2014).
6. Gentile, V., Schrijer, F.F.J., van Oudheusden, B.W, Scarano, F., Afterbody Effects on Axisymmetric Base Flows. 53rd AIAA Aerospace Sciences Meeting. American Institute of Aeronautics and Astronautics (2015).
7. Lynch, K.P., Scarano, F.: An efficient and accurate approach to MTE-MART for time-resolved tomographic PIV. Exp. Fluids. **56** (2015).
8. Atkinson, C., Soria, J., An efficient simultaneous reconstruction technique for tomographic particle image velocimetry. Exp. Fluids. **47** (2009).
9. Discetti, S., Natale, A., Astarita, T., Spatial filtering improved tomographic PIV. Exp. Fluids. **54** (2013).
10. Westerweel, J., Scarano, F., Universal outlier detection for PIV data. Exp. Fluids. **39** (2005).
11. Pröbsting, S., Scarano, F., Bernardini, M., Pirozzoli, S., On the estimation of wall pressure coherence using time-resolved tomographic PIV. Exp. Fluids. **54** (2013).
12. Ghaemi, S., Ragni, D., Scarano, F., PIV-based pressure fluctuations in the turbulent boundary layer. Exp. Fluids. **53** (2012).
13. De Kat, R., van Oudheusden, B.W., Instantaneous planar pressure determination from PIV in turbulent flow. Exp. Fluids. **52** (2011).
14. Charonko, J.J., King, C. V, Smith, B.L., Vlachos, P.P., Assessment of pressure field calculations from particle image velocimetry measurements. Meas. Sci. Technol. **21** (2010).
15. Deprés, D., Reijasse, P., Dussauge, J., Analysis of unsteadiness in afterbody transonic flows. AIAA J. **42** (2004).
16. Meliga, P., Reijasse, P., Unsteady Transonic Flow Behind An Axisymmetric Afterbody Equipped With Two Boosters. 25th AIAA Applied Aerodynamics Conference. American Institute of Aeronautics and Astronautics (2007).
17. Weiss, P.-E., Deck, S.: Control of the antisymmetric mode (m = 1) for high Reynolds axisymmetric turbulent separating/reattaching flows. Phys. Fluids. **23** (2011).
18. Bitter, M., Hara, T., Hain, R., Yorita, D., Asai, K., Kähler, C.J., Characterization of pressure dynamics in an axisymmetric separating/reattaching flow using fast-responding pressure-sensitive paint. Exp. Fluids. **53** (2012).